Telecommunication through geological layers using seismic waves
La télécommunication à travers les couches géologiques par l'utilisation des ondes sismiques

Christina Akleh[1,2,*], *Hervé* Chauris[2], *Bruno* Figliuzzi[2], *Renaud* Fallourd[1], and *Paul* Hardouin[3]

[1]Agence national pour la gestion des déchets radioactifs, Andra, France
[2] Centre de recherche de Mines Paris – PSL université, Statistique et Images (STIM), France
[3] Seismic Smart Solutions, S[3], France

Abstract. This work investigates the feasibility of transmitting information through geological layers using seismic waves. It is a part of developing wireless underground communication alternatives for the Internet of Underground Things (IoUT). Experiments were conducted at the ANDRA Underground Research Laboratory to transmit for the first time data from 490 m depth to the surface. To that end, we used about 20–25 wavelengths at frequencies [103 Hz -124 Hz] with Vp = 2500 m/s. These small size data (17×11-pixel image) were encoded using the Hamming (7, 4) code. Each pixel was converted to frequency activations and transmitted from an underground tunnel to 30 geophones deployed on the surface. Time–frequency analysis enabled identification of emitted frequencies. Using threshold-based frequency detection followed by Hamming error corrector, the transmitted image was successfully reconstructed. Stacking five repeated experiments significantly improved the signal-to-noise ratio and reducing pixel errors. Although only a few errors were observed in this small test case, larger and more complex datasets are expected to better challenge the robustness of the Hamming code. These findings show the potential seismic waves as a viable communication method in deep geological environments. It also emphasizes the necessity for adaptive decoding algorithms and further testing with larger images.

Résumé. Cette étude examine la possibilité de transmettre des informations à travers des couches géologiques en utilisant des ondes sismiques. Elle se rattache au développement de méthodes de communication sans fil pour l'Internet des objets souterrains (IoUT). Des expériences ont été menées au Laboratoire de Recherche Souterrain de l'Andra pour transmettre, pour la première fois, des données depuis 490 m de profondeur jusqu'à la surface. Pour ce faire, 20–25 longueurs d'onde P ont été utilisées pour des fréquences de 103 à 124 Hz avec Vp=2500 m/s. Les données, incluant une image de 17×11 pixels, ont été codées avec un code Hamming (7,4), converties en activations de fréquence et transmises vers 30 géophones en surface. L'analyse temps-fréquence a permis d'identifier les fréquences émises et, grâce au décodage Hamming, l'image a été correctement reconstituée. La somme de cinq expériences répétées a amélioré le rapport signal-bruit et réduit les erreurs de pixels. Bien que ce

* Corresponding author: christina.akleh@minesparis.psl.eu

test ait révélé peu d'erreurs, des ensembles de données plus grands et complexes permettront d'évaluer plus précisément la robustesse du code. Ces résultats confirment le potentiel des ondes sismiques comme moyen de communication en milieu géologique profond et soulignent la nécessité de méthodes de décodage adaptatives ainsi que de tests supplémentaires avec des images plus volumineuses.

1 Introduction

The Internet of underground Things (IoUT) uses burried sensors and communication modules to monitor subsurface conditions in areas such as agriculture, geotechnical investigations, and sub-surface infrastructure monitoring [1, 2, 3, 4, 5] . Since cables are challenging and costly to install, IoUT systems primarily rely on wireless underground communication (WUC) [6, 7]. The performance of these wireless transmitters therefore becomes critical for reliable data transmission through soil. Conventional underground communication involves electromagnetic (EM) or magnetic induction (MI) signals, although both encounter significant challenges in soil. Therefore an alternative wireless underground communication method, based on seismic waves, has been proposed [7, 8].

The use of seismic waves is widely recognized in geophysics and geotechnical applications using surface wave analysis, seismic reflection, and refraction [2]. Nevertheless, it is still uncommon to use them for communication such as data transmission. The premise of conventional seismic communication systems is that information (such as letters, numbers, and even images) is encoded, transformed into mechanical vibrations, transmitted through a communication channel. Then, it is detected by sensors such as geophones or accelerometers and then decoded to retrieve the original message (Figure 1) [2]. In circumstances where electromagnetic communication is unreliable or impossible, seismic waves present a promising alternative since soil effectively transmits low-frequency vibrations.

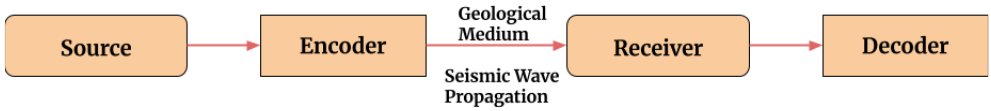

Figure 1 : Schematic of the communication model.

Vibration-based wireless underground communication (WUC) system is one bio-inspired example [7]. In this approach, text or image files are transmitted via the soil using seismic signals produced by tiny vibrating sources (inspired by mole-rat drumming activities). Accelerometers recover binary-encoded signals. Experiments showed that text and images could be transmitted successfully at distances of up to 80 cm. However the quality was affected by noise, soil variability, and transmission loss.

Animals like elephants also use seismic communication naturally. Their low-frequency (10–40 Hz) and high-amplitude vocalizations may travel large distances through the ground. In some modeled cases, these signals travel up to 32 km equivalent to roughly 100 to 320 wavelengths. Elephants can communicate over kilometers and recognize its surroundings due to these signals [9, 10]. The potential of ground-bone communication lines is supported by their capacity to identify very small seismic vibrations.

Besides biological systems, seismic communication has been proven on larger scales [11]. In one study, vibroseis sources and geophones were used to send Morse-coded seismic signals in an urban setting. Despite interference from footsteps, elevators, and electromagnetic equipment, Segmented Correlation Technology for Multiple Channels

(SCTMC) allowed for successful signal extraction at distances of up to 60 m, which could be extended to 120 m using relays [11]. It corresponds to roughly 4 to 8 seismic wavelengths.

Although issues like noise, attenuation, and soil heterogeneity continue to be major research challenges, the result of these studies indicates the feasibility of the use of seismic waves as a practical communication medium in subsurface and interference-prone situations [5, 8].

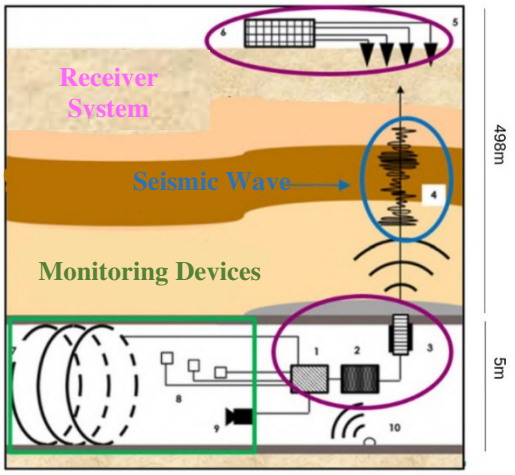

Figure 2: Simplified schematic diagram of the SeisCom wireless transmission concept. The vertical axis is zoomed in on the deeper section, corresponding to the 5 m-diameter tunnel.

In this work, experiments have been conducted with the support of seismic smart solution at ANDRA Underground Research Laboratory (URL) of Meuse/Haute-Marne center. In the context of the development of the French Industrial Centre for Geological Disposal (Cigéo) for radioactive waste, the URL aims at further improving the knowledge on the Callovo-Oxfordian host rock characteristics, its ability to contain radioactive elements and the capacity to construct underground structures within this rock [12]. It focuses on studying the properties of clay, understanding interactions between disposals facilities and the surrounding geology, and refining construction methods [12].

The goal of the experiments was to assess the effectiveness and the reliability of telecommunication using seismic waves for underground monitoring at a depth of 490 meters. The experiment setup includes 30 geophones deployed on the surface and two seismic source position (borehole and on the ground of the tunnel) at 490 meters in the URL (Figure 2).

A SeisMovie seismic source, which is a low energy piezoelectric vibrator, was used to generate signals from the 490 meters depth to the surface [13]. This setup yields to produce repeatable signals enabling accurate time-frequency analysis of the transmission. During these experiments the first transmission of encoded from 490 meters depth to the surface was established. The transmitted information included physical parameters such as temperature values as well as images. Various encoding and decoding methods were tested, including Morse code, frequency modulation, and Hamming (7, 4). The analysis presented here focuses specifically on transmission of small size image encoded using the Hamming (7, 4) approach.

The article is organized as follows. The methodology is first detailed in section 2. The results of the transmission and reconstruction of an 11×17-pixel image are presented in section 3. Future results directions are discussed in the final section.

2 Methodology: Hamming code (7,4)

We describe in this section the encoding of the image performed prior to its transmission, based on a Hamming code [14].Hamming codes are a class of error-correcting codes designed to detect and correct single-bit errors in transmitted data. For a (7, 4) Hamming code, 4 data bits d = [*d1, d2, d3, d4*] are encoded into a 7 bits code **c** = [*c1, c2, c3, c4, c5, c6, c7*] using a generator matrix (**G**), defined as:

$$\mathbf{G} = \begin{bmatrix} 1\,0\,0\,0 \\ 0\,1\,0\,0 \\ 0\,0\,1\,0 \\ 0\,0\,0\,1 \\ 1\,1\,0\,1 \\ 0\,1\,1\,1 \\ 1\,0\,1\,1 \end{bmatrix} \tag{1}$$

The codeword **c** is computed as **c = G .d**. Upon reception, a syndrome **s = H.c** is calculated using the parity-check matrix **H**, defined as:

$$\mathbf{H} = \begin{bmatrix} 1\,0\,1\,0\,1\,0\,1 \\ 0\,1\,1\,0\,0\,1\,1 \\ 0\,0\,0\,1\,1\,1\,1 \end{bmatrix} \tag{2}$$

Columns 1, 2, 4 are occupied by the parity bits (p_i), and 3, 5, 6, 7 by the data bits (d_i). With parity bits

$$p_1 = d_1 \oplus d_2 \oplus d_4, \quad p_2 = d_1 \oplus d_3 \oplus d_4, \quad p_3 = d_2 \oplus d_3 \oplus d_4 \tag{3}$$

where $\oplus$ is the bitwise XOR operator.
The syndrome **s** is critical to error detection and localization. If **s** = 0 so the codeword is valid. However, If **s** $\neq$ 0, at least one transmission error has occurred. In the presence of a single error, the syndrome uniquely identifies the position of the error, allowing it to be corrected.

In this study, the choice of the (7, 4) Hamming code is justified by the fact that the image contains only 4 colors, so 4 bits are sufficient to encode any pixel. Additionally, the number of frequencies that can be transmitted simultaneously by the source is limited, which favors using a Hamming code with a small number of bits. Since they serve as a robust single-bit error correction in applications including memory systems, data storage, and communication networks, Hamming codes are widely used for their reliability and simplicity [15].

3 Transmission application

The May 2025 experiment focused on transmitting data from 490 m-deep tunnel to the surface. Here we will analyse a 17x11 pixel Bidon image as a baseline to validate direct encoding and decoding (Figure 3). Each pixel was encoded individually using the Hamming (7, 4) approach, resulting in direct pixel-by-pixel transmission.

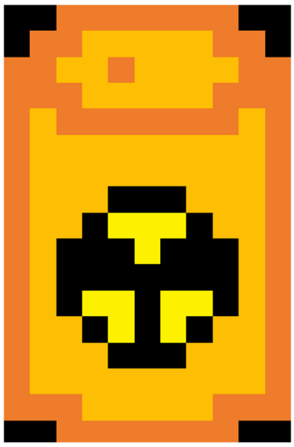

Figure 3 : Original 17x11 pixels image transmitted with 4 colors.

A SeisMovie type seismic source was used in the on-ground position to generate controlled vibrations [13]. Each pixel was encoded using Hamming (7, 4) approach. The resulting encoded bits were mapped to frequencies: a bit '1' activates its allocated frequency, while a '0' leaves it inactive. Frequencies from 103 to 124 Hz, with an increment of 2 Hz, 3 Hz and 4 Hz, were selected to avoid the 50 Hz electrical noise and its harmonics which would otherwise mask the transmitted frequencies (Figure 4). The bit sequence 01010 corresponds to the black color (Table 1).

Table 1 : Set of frequencies encoding the color black, represented by the Hamming code 0101010.

Frequency(Hz)	103	106	108	112	115	118	121
Bit	0	1	0	1	0	1	0

The choice of these specific frequencies depended on the seismic source position, based on prior studies showing that certain bands propagate more efficiently from this position. The composite signal, containing all activated frequencies, was transmitted for 1 s per pixel with a sampling rate of $\Delta t = 1$ ms from the 490 m deep tunnel to surface geophones. A total of 28 Sercel SG-5 vertical geophones and two 3-component geophones were installed. However, only 27 of the SG-5 geophones were used in the analysis. A specific marker "fix" was used to mark the end of each row in the image. It is transmitted with a dedicated mono-frequency (124), distinct from the data sequence, ensuring accurate reconstruction of the transmitted image. The total duration of the transmission is about 204 s. This experiment was repeated five times.

In order to estimate and adjust the relative time shifts between geophones, time alignment was performed by cross-correlating each trace with a chosen reference trace. The detected shifts were all smaller than sampling rate. After alignment, the 27 geophone traces were stacked for each experiment to enhance the signal-to-noise ratio.

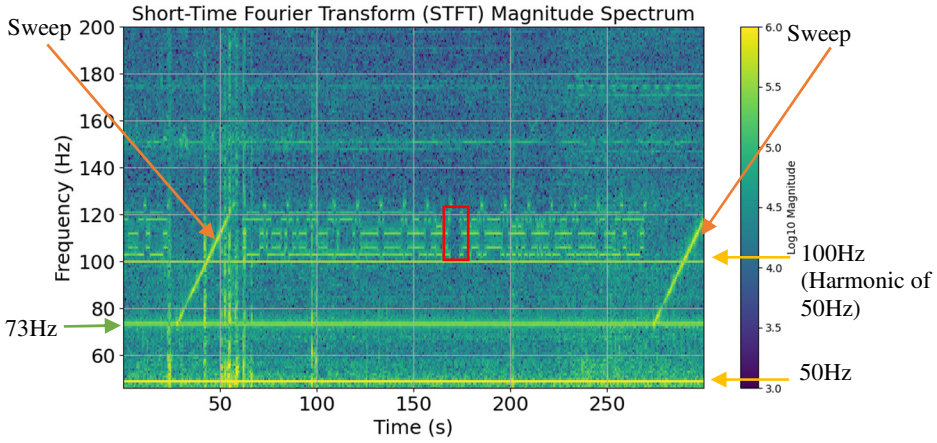

Figure 4: The Short-Time Fourier Transform (STFT) spectrogram showing the transmission of the Bidon image (1 s per pixel) for a single experiment. Frequency sweeps (orange arrows) mark the start and end of the transmission, and a 4-s gap is highlighted in red box. A strong, continuous 50 Hz signal, corresponding to the DC component, and its harmonics at 100 Hz are visible in all spectrograms (yellow arrows). A persistent 73 Hz signal of unknown origin is also present (green arrow). The background noise is not stationary, showing vertical stripes and peaks in the frequency domain, likely due by intermittent site activities such as elevators, vehicles, and machinery.

The stacked trace of a single Bidon image transmission experiment was divided into overlapping windows of 1000 samples with a 500-sample step and detrended by subtracting the mean to remove the DC offset. A Hanning window was applied to each segment before computing its Fourier transform. This produced the short-time Fourier transform, with time vectors obtained at the middle of each window and magnitudes shown on a logarithmic scale, offering a clear frequency-time view of the transmitted signals.

The detection of the start and end times for each experiment was determined using a Short-Time Fourier Transform (STFT) on a stack trace of all geophones (Figure 4). Each experiment was preceded and followed by a frequency sweep from 73 to 125 Hz, providing clear temporal boundaries for picking. Each pixel was transmitted for 1 s. The emitted frequencies identified from the spectrogram.

The total duration of image transmission is 208 s slightly longer than the expected 204 s for the 17 × 12 pixel configuration (including the “fix” mark). A 4-second gap occurred after 108 s, observed in the five repeated experiments, during which no frequencies were emitted. This delay likely resulted from the DAQ card requiring extra time to buffer data before transfer to the amplifier.

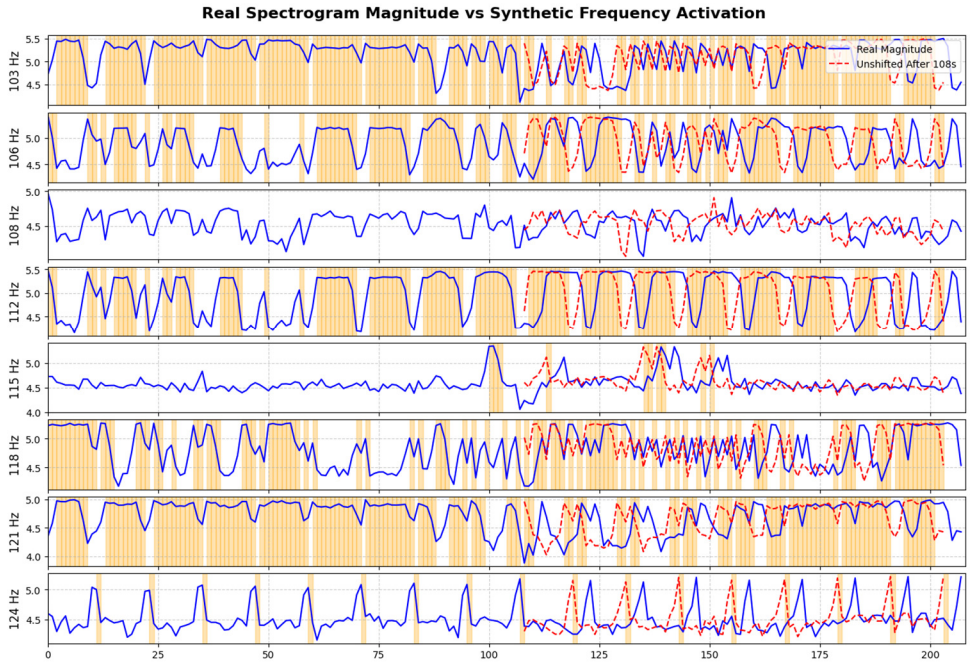

Figure 5: Comparison of the recorded spectrogram magnitudes (blue solid line) obtained from the STFT for each emitted frequency with the expected encoded bit frequency activations (orange boxes) during 1-s pixel transmissions. A red dashed curve indicates the 4-s time shift observed after 108 s in the spectrogram, after applying this correction, the expected activations (orange) and the shifted reference (red) are superposed.

To analyze the observed 4-second gap, the recorded spectrogram was compared with the expected frequency activations for each 1 s transmission of individual pixels. The measured signal magnitudes are shown as a blue solid line, while the expected encoded bit activations are represented as orange boxes (Figure 5). Up to 108 s, the measured and expected activations closely matched, indicating accurate transmission and timing. Beyond this point, a systematic 4-second delay appeared in the measured signals. This shift is highlighted by a red dashed curve, representing the adjusted signal after applying a 4-second correction to align the spectrogram with the expected activations. After this correction, the expected activations (orange) and the time-shifted measured signals (red) were superposed, confirming the timing discrepancy.

Based on this analysis, the four erroneous codewords occurring between 108-112 s due to the delay were removed. Each 1-second time step was used to extract the magnitude along the vertical axis of the spectrogram. A manual threshold of 4.8 was then applied to classify each frequency as active (1) or inactive (0), allowing the reconstruction of the transmitted bit sequences.

The binary sequences were passed through a Hamming error-correction function to fix single-bit errors if it exits. Following decoding, the bitstream was reshaped into a two-dimensional image array, which was then converted to RGB colors and compared to the original Bidon image.

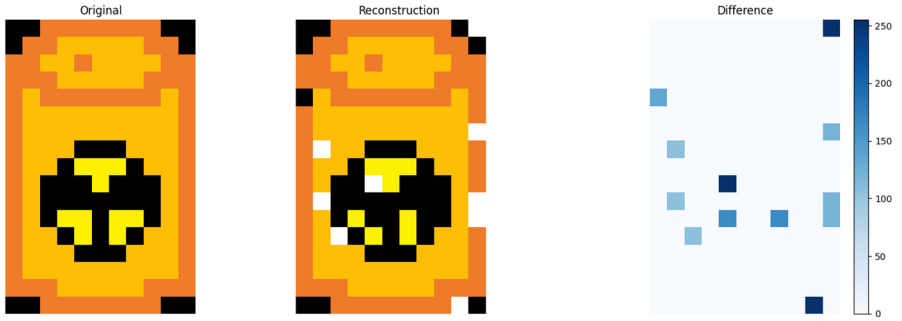

Figure 6 : Original image (left), reconstructed image after correcting the 4-second delay (middle), and difference image highlighting pixel discrepancies (right) for a single Bidon image transmission at 1 second per pixel.

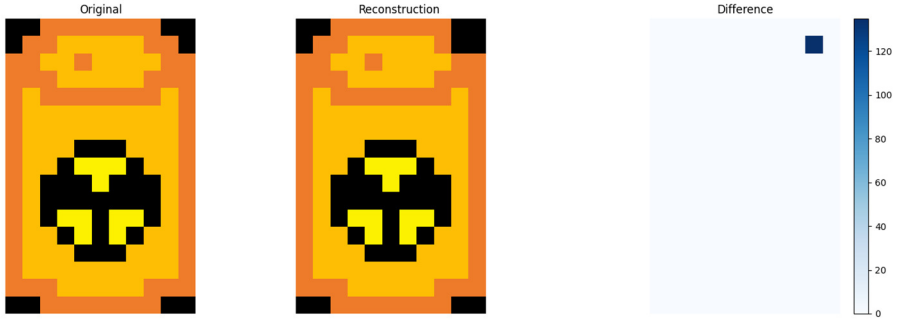

Figure 7: Same as Figure 6 but after stacking five repeated transmission.

Figure 6 shows that the reconstructed image closely matched the original, confirming the successful encoding, transmission, and decoding of the Bidon image. The fix-marker codewords (value 15) appear as white pixels in the decoded result. For a single experiment, the reconstruction was generally accurate, with only eight pixels incorrectly decoded out of the 17×11-pixel image as showed in the difference panel. This may be due to the use of a single threshold for all frequencies, which can cause misdetections because their amplitudes vary.

To evaluate the stability of the method, the same experiment was repeated five times under similar conditions. When the five recordings were stacked, the overall signal-to-noise ratio (SNR) increased by $\sqrt{5}$ (5 repeated experiments), which enhanced the accuracy of frequency detection during the decoding phase. As shown in Figure 7, the stacked reconstruction produced only one incorrect pixel out of the 204 transmitted pixels, representing a significant improvement compared to any individual experiment.

Despite these positive outcomes, the reconstruction workflow still presents certain limitations. Most importantly, it relies on a single fixed threshold applied uniformly across all experiments and all frequencies, an assumption that does not always capture variations in signal amplitude caused by changes in source performance, or background noise. At the present making the decoding workflow semi-automated.

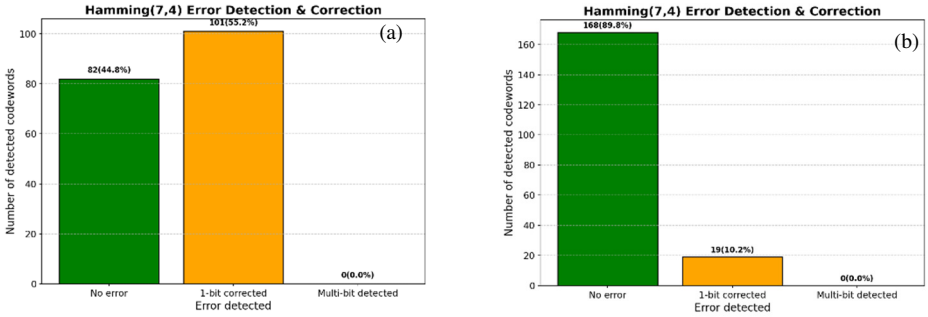

Figure 8: Error detection and decoding results for the Bidon image transmission. The left panel shows the pixel by pixel decoding result for a single experiment, including correctly decoded pixels and single-bit errors. The right panel shows the stacked result from five repeated experiments, where the total number of decoding errors is reduced due to the improvement of the signal-to-noise ratio.

Figure 8 shows that, for a single experiment of the Bidon image transmission, the Hamming (7, 4) code detected and corrected a single-bit error in 101 out of 183 pixels (55%) (white pixels corresponding to fix markers are not included), while 0% of multi-bit errors occurred and 45% of pixels were correctly decoded directly. For the stack of five repeated experiments, the code detected and corrected single-bit errors in 19 out of 187 pixels (10%), with 0% multi-bit errors, and 168 out of 187 pixels (90%) were correctly decoded directly. The relatively small number of error corrections is mainly due to the improved the SNR after the stacking, thus the improvement of the frequency detection and decoding. In a single experiment, the Hamming code plays a significant role in correcting single-bit errors.

However, the test case is simple: a small 17×11 image with only four colors, resulting in relatively low information density. Since complex images, with more colors, larger size, or greater pixel variation, provide a wider variety of codewords, increasing the likelihood that noise may cause errors Hamming (7, 4) cannot correct. This leads to more decoding errors and provides a more realistic assessment of the code's performance under typical data conditions. Furthermore, larger images can not be transmitted pixel by pixel, therefore compression techniques and labelling must also be tested to in order to guarantee efficient transmission. Additionally, future work should quantify how the number of detected errors varies with the number of geophones and test the code with more complex images. This analysis will be essential for assessing the robustness and scalability of Hamming-based decoding in seismic communication systems.

4 Conclusion

In May 2025, the first transmission of an image from underground (490 m depth) to the surface using seismic waves occurred. Using Hamming (7, 4) code, it validated through the successful encoding, transmission, and reconstruction of a small 17×11 image. The studies showed that, under controlled conditions and limited data size, the Hamming code played a determined role in correcting errors. Stacking multiple repetitions further improved the reconstruction quality by increasing the signal-to-noise ratio, which also enhanced frequency detection and error correction. However, due to the simplicity of the test case, the error-correction capabilities of the Hamming code were not fully challenged. Larger and more complex images, with higher pixel variability or more colors, are expected to generate more transmission errors, providing a more comprehensive evaluation of the method's robustness. Future work should therefore investigate error rates as a function of both image size, the number of geophone and the duration of the transmission to better evaluate scalability and reliability. Overall, the results confirm the potential of seismic-based data transmission while highlighting key challenges for improving and validating this technique for real underground

communication applications. Advanced strategies, including adaptive detection thresholds and machine-learning-based frequency classification, will be explored to enhance robustness and automation.

References

[1] I. F. Akyildiz and E. P. Stuntebeck, "Wireless underground sensor networks: Research challenges," *Ad Hoc Networks,* vol. **4**, no. 6, pp. 669-686, 2006.

[2] T. Jiang, "Feasibility of electromagnetic vibroseis seismic wave communication and design of carrier signal," *Pure Appl. Geophys.,* vol. **179**, no. 2, pp. 765-775, 2022.

[3] A. Salam and S. Shah, "Internet of Things in Smart Agriculture: Enabling Technologies," in *IEEE 5th World Forum on Internet of Things (WF-IoT)*, (2019).

[4] M. C. Vuran, A. Salam, R. Wong and S. Irmak, "Internet of underground things in precision agriculture: Architecture and technology aspects," *Ad Hoc Networks,* vol. **81**, pp. 160-173, (2018).

[5] A. Salam and S. Shah, "Urban Underground Infrastructure Monitoring IoT: The Path Loss Analysis," in *IEEE 5th World Forum on Internet of Things (WF-IoT)*, (2019).

[6] I. F. Akyildiz, Z. Sun and M. C. Vuran, "Signal propagation techniques for wireless underground communication networks," *Phys. Commun.,* vol. **2**, no. 3, pp. 167-183, (2009).

[7] Y. Zhong and J. J. Tao, "Bio-inspired vibrational wireless underground communication system," *Rock Mech. Geotech. Eng.,* vol. **14**, no. 4, pp. 1042-1051, (2022).

[8] N. Saeed, M.-S. Alouini and T. Y. Al-Naffouri, "Toward the Internet of Underground Things: A systematic survey," *IEEE Communications Surveys & Tutorials,* vol. **21**, no. 4, (2019).

[9] G. R. H., C. E. O'Connell-Rodwell and S. L. Klemperer, "Seismic waves from elephant vocalizations: A possible communication mode?," *Geophys. Res. Lett.,* vol. **31**, no. 11, (2004).

[10] C. E. O'Connell-Rodwell, "Keeping an “ear” to the ground: seismic communication in elephants," *Physiology, (*2007).

[11] Y. Jiang, "Application of the segmented correlation technology in seismic communication with Morse code," *Appl. Sci.,* vol. 11, no. 4, p. 1947, 2021.

[12] M.-C. Dupui and F.-M. Gonnot, “Projet cigéo centre industriel de stockage réversible Profond de déchets radioactifs en meuse/haute marne,” Andra, (2013).

[13] J. Cotton, L. Michou and E. Forgues, "Continuous land seismic reservoir monitoring of thermal EOR in the Netherlands," (2013).

[14] R. W. Hamming, "Error detecting and error correcting codes," *The Bell system technical journal,* vol. **29**, no. 2, pp. 147-160, (1950).

[15] S. Charoghchi, Z. Saeidi and S. Mashhadi, “Integer wavelet transform-based secret image sharing using rook polynomial and Hamming code with authentication,” *CAAI Trans. Intell. Technol.,* vol. **9**, no. 6, pp. 1435-1450, (2024).